flection. For matte surfaces like those of the standard color chips, the second reflectance component dominates. The

dichromatic reflection model for inhomogeneous materials

like plastics suggests that under all illumination and view-

ing geometries the spectral reflectance function can be ex-

pressed as the weighted sum of two functions: the constant

interface reflectance function and the body reflectance func-

tion. 4,10 Tominaga and Wandell 11 and Lee et al. 12 examined

the adequacy of this standard dichromatic reflection model,

and Tominaga¹³ proposed an extension of the dichromatic

model in order to describe the surface-spectral reflectances

reflection model is that the geometric factor on illumina-

tion and viewing and the spectral factor on interface and

body reflectances are separable. In previous reports we

specified only the spectral factor and treated the geomet-

ric factor as being included in the weighting coefficients

of the spectral reflectance functions. However, models with-

out geometric specification are insufficient for generating computer graphics images of three-dimensional objects in

a scene, because rendering three-dimensional objects requires the modeling of three-dimensional light reflection

This report describes light reflection models adequate for generating computer graphics images of object surfaces of three different types of materials. In the following sec-

tions, we first show three types of dichromatic reflection

models for describing surface-spectral reflectances of a va-

riety of materials. Next, we determine the geometric

weights to complete the total dichromatic light reflection

models by combining the geometric and wavelength fac-

tors. Finally, we demonstrate realistic images of reflec-

tive objects generated by the three types of models for the

One of the most important properties of the dichromatic

of a larger variety of materials.

from surfaces.

different materials.

Dichromatic Reflection Models for Rendering Object Surfaces*

Shoji Tominaga†

Department of Engineering Informatics, Osaka Electro-Communication University, Neyagawa, Osaka 572, Japan

We describe light reflection models adequate for generating realistic images of reflective object surfaces. The surface-spectral reflectance of an object varies with the geometry of illumination and viewing. This function also depends on the object's material composition. First we show three types of dichromatic reflection models for describing surface-spectral reflectances of a variety of materials. The Type I model for inhomogeneous dielectric materials, such as plastics, assumes that surface reflection consists of two additive components, the body reflection and the interface reflection that is independent of wavelength. The Type II model for cloths and papers allows wavelength-dependent interface reflection. The Type III model for metals has two interface reflection components. Next we determine the geometric factors of illumination and viewing angles, which so far had been left as undetermined weighting coefficients to the spectral components. The intensity distribution of the reflected light from a surface is formulated by referring to reflection models in computer graphics. Thus, reflective object surfaces of most materials can be rendered using these three types of dichromatic models. Finally, sample images for different surface types are generated.

Journal of Imaging Science and Technology 40: 549-555 (1996)

Introduction

Modeling the reflection properties of object surfaces is crucial in color measurement and in color applications. In computer graphics, reflectance models have been used for generating realistic images. 1-3 Machine vision applications often require reflectance models for image analysis and object recognition. 4.5 A reflectance model has been used for classifying wood-surface features in wooden products. 6 Moreover, a dichromatic linear model has been utilized for realizing color constancy. 7.8 In printing applications, a reflectance model is used for simulating the color printing process. 9

The surface-spectral reflectance of an object varies with the illumination and viewing geometry. This function also depends on the object's material composition. The reflectance is usually decomposed into two components: interface (specular) reflectance and body (diffuse) reflectance. The interface reflection occurs at the interface between the object's surface and the air. Reflection from homogeneous materials like metals consists mostly of the interface re-

Dichromatic Reflection Models The Standard Model (Type I). Figure 1 sketches the reflection process that applies to nonconducting materials called inhomogeneous dielectric materials. The radiance $Y(\theta,\lambda)$ of light reflected from a surface is a function of the wavelength λ and the geometric parameters θ , including the illumination.

tion direction angle, the viewing angle, and the phase angle. The dichromatic reflection model describes the reflected light as the sum of interface and body reflections,

 $Y(\theta, \lambda) = c_I(\theta) L_I(\lambda) + C_B(\theta) L_B(\lambda), \tag{1}$

where the terms $L_I(\lambda)$ and $L_B(\lambda)$ are the spectral power distributions of the interface and body reflection components, respectively. These components remain unchanged as the geometric angles vary. The weights $c_I(\theta)$ and $c_B(\theta)$ are the geometric scale factors.

The body reflection is caused by light scattering among the pigments in the colorant layer. Therefore, the spatial

Original manuscript received June 11, 1996. Revised September 13, 1996.

^{*} Presented in part as the paper entitled "Using Reflectance Models for Surface Estimation" at the 3rd IS&T/SID Color Imaging Conference, November 7–10, 1995, Scottsdale, Arizona.

[†] IS&T Member

^{© 1996,} IS&T-The Society for Imaging Science and Technology

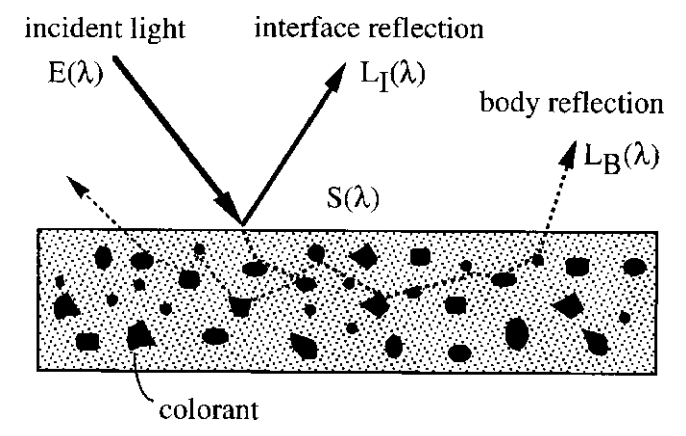


Figure 1. Reflection model in an inhomogeneous dielectric material.

distributions of these two reflection components are quite different. The direction of light scattered through interface reflection is restricted to a narrow angular interval in much the same way as a mirror reflects incident rays. Conversely, the light scattered by the body reflection emerges equally in all directions.

Let us express the model in terms of surface-spectral reflectances. The reflectance is defined as the ratio of the radiance $Y(\theta, \lambda)$ by the given surface element to the radiance $Y_w(\theta, \lambda)$ by a perfect reflecting diffuser illuminated in the same way as the given surface.

$$S(\theta, \lambda) = Y(\theta, \lambda) / Y_{w}(\theta, \lambda). \tag{2}$$

This quantity is called the *radiance factor* in the radiometric term. ¹⁴ On the other hand, let $E(\lambda)$ be the spectral power distribution (irradiance) of the incident light. The radiance of reflected light is proportional to the incident irradiance as $Y(\theta, \lambda) \propto E(\lambda)$. Especially the relationship for the perfect reflecting diffuser is given by the simple formula $Y_w(\theta, \lambda) = E(\lambda)/\pi$. The spectral reflectance is then written as

$$S(\theta, \lambda) = \pi Y(\theta, \lambda) / E(\lambda). \tag{3}$$

The constant π is omitted when the relative values of surface-spectral reflectances are analyzed in this study.

Because the dichromatic reflection occurs, the spectral reflectance can be expressed as the sum of two components,

$$S(\theta, \lambda) = c_I(\theta) S_I(\lambda) + c_B(\theta) S_B(\lambda), \tag{4}$$

where $S_I(\lambda)$ and $S_B(\lambda)$ are the surface-spectral reflectances for the interface and body components, respectively. The standard model incorporates the so-called neutral interface reflection (NIR) (or constant interface reflection) assumption, which states that the interface reflection component $S_I(\lambda)$ is constant over the band of visible wavelengths as $S_I(\lambda) = S_I^c$ and thus may be eliminated from Eq. 4:

$$\begin{split} S(\theta,\lambda) &= c_I(\theta) S_I^c + c_B(\theta) S_B(\lambda) \\ &= c_I'(\theta) + c_B(\theta) S_B(\lambda). \end{split} \tag{5}$$

The standard dichromatic reflection model is valid for plastics, paints, ceramics, vinyls, tiles, fruits, leaves, and woods. $^{11-13}$

Figure 2 shows a set of normalized curves of the surface-spectral reflectances from a red plastic cup. All the reflectance curves are normalized to unit length. The set of curves marked with plus symbols represents the spectral

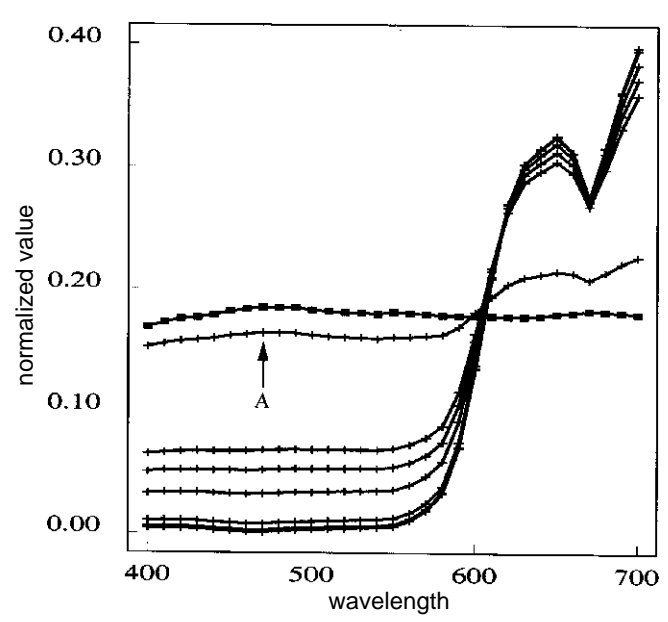


Figure 2. Normalized curves of the observed surface-spectral reflectances from a red plastic cup.

reflectances measured at nine different points on the uniformly colored surface of the cup. The curve marked A, which is close to a straight line, represents the observations made in a highlight area. The validity of the standard model can be confirmed for these reflectance curves by testing the two conditions of "two-dimensionality" and "constant interface reflectance" based on Eq. 5. This process is as follows: First, the principal component patterns of the set of curves are extracted, using the singular value decomposition (SVD) method. Because the variance for only the first two principal components exceeds 99.9%, the curves are regarded as being two-dimensional. Second, the first two component patterns are fitted to a straight line by linear regression. The nearly straight line with squares in Fig. 2 shows the fitting result that approximates a constant reflectance.

The Extended Model for Cloth and Paper (Type II). Some cloths and papers are described by the second type of dichromatic reflection model. Tominaga 13 first defined this type for rayon satin cloth and polyester satin cloth. Usui and Imamura⁹ recently found this type to be adequate for describing the surface reflection of printed papers. Figure 3 shows the surface-spectral reflectances observed at a patch of cyan solid color printed on paper. The normalized curves of the reflectances are depicted in a three-dimensional view as a function of the viewing angle, where the angle of incidence of illumination is fixed at 8° , while the viewing angle varies in the range of $-8^\circ-+35^\circ$. Note that the spectral reflectance curves around the mirrored direction of +8° are not constant with respect to wavelength, although a strong gloss had appeared on the paper surface at that angle. Constant specular reflectance could not be observed at any angle. These reflectance curves satisfy the first condition of two-dimensionality, but the second condition of "constant interface reflectance" is not satisfied.

Surface-spectral reflectances for such materials are dichromatic, but the specular reflections at the interface include no illuminant component. This kind of surface-spectral reflectance function is described as the generalized dichromatic reflection model of Type II,

$$S(\theta, \lambda) = c_I(\theta) S_I(\lambda) + c_R(\theta) S_R(\lambda), \tag{6}$$

where the interface reflectance component $S_I(\lambda)$ is not necessarily constant with respect to wavelength.

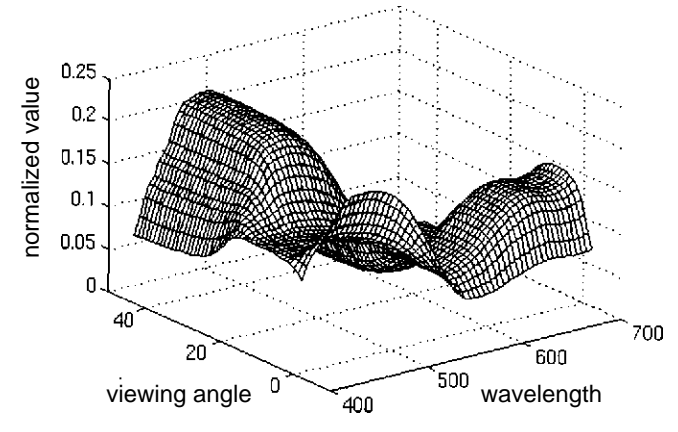


Figure 3. 3D view of the observed reflectances from a color patch painted with a cyan solid ink on an art paper.⁹

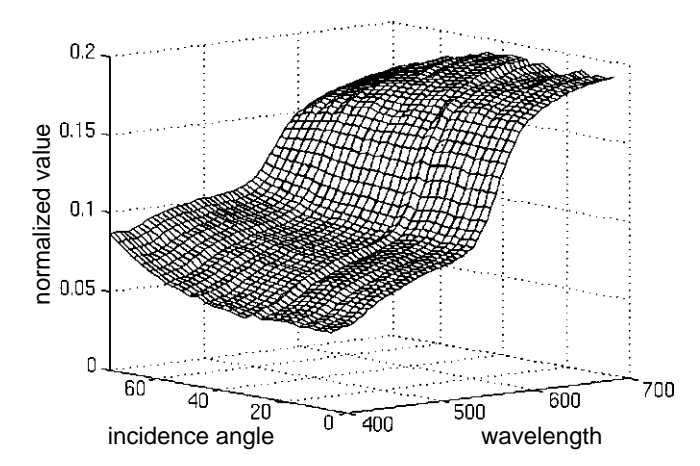


Figure 4. 3D view of the observed reflectances from a metal plate of copper.

The Extended Model for Metals (Type III). Metals have quite different reflection properties from inhomogeneous materials, because they have only interface reflection. If the surface is stainless, the body reflection of the reflected light is negligibly small. A sharp specular highlight is observed only at the viewing angle of the mirrored direction. This type of reflection obeys Fresnel's law, ¹⁵ and the surface-spectral reflectance function depends on the incident angle of illumination.

Figure 4 shows the surface-spectral reflectances observed from a plate of copper. The normalized curves of the spectral reflectances are depicted in a three-dimensional view to show the influence of changing the incident angle in the range of 5° to 75°. The viewing angle has always been set to the mirrored direction in order to measure only the specular reflection. It is easily predicted that as the angle approaches the grazing angle of 90°, the shape of the spectral reflectance tends to become constant over the range of visible wavelengths (white). The SVD shows that the surface-spectral reflectances of copper are described by two interface reflectance components, one of which is the constant spectral reflectance. The same properties were shown for several other metals. ¹³

The dichromatic reflection model of Type III is defined for approximating the surface-spectral reflectance function of a metal as

$$S(\theta, \lambda) = c_{I1}(\theta)S_I(\lambda) + c_{12}(\theta)S_{I2}^c$$

= $c_{I1}(\theta)S_I(\lambda) + c'_{I2}(\theta)$. (7)

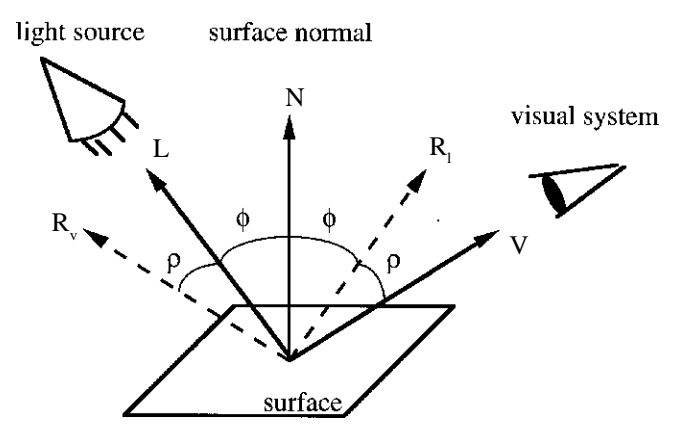


Figure 5. Reflection geometry.

The right-hand side in Eq. 7 represents two interface reflection components. The first term corresponds to the specular reflection at the normal incidence. The second term, which is constant over the visible wavelength range, corresponds to the grazing reflection at the horizontal incidence.

Total Light Reflection Models for Rendering Objects

In this section we determine the geometric factor, which has been left undetermined as the weighting coefficients in the dichromatic reflection models. The intensity distribution of the reflected light is analyzed, and the total three-dimensional light reflection models are defined for rendering reflective objects of the three types of classified materials.

Type I Model. The body reflection component occurs for light that crosses the interface between the object's surface and the air and causes scattering among the pigments in the colorant layer as shown in Fig. 1. Because this scattered light is observed only after it crosses the interface again into the air, the body component does not have strong directed components, but emerges with equal strength in all directions. Therefore, it is assumed to obey Lambert's law, which states that the intensity of reflected light is independent of the viewing direction and proportional to the cosine of the angle of the incident light.16 Figure 5 depicts the reflection geometry, where N is the surface normal, L is the incident light vector, and V is the viewing vector. Moreover, \mathbf{R}_1 and \mathbf{R}_v are, respectively, \mathbf{L} and V mirrored about N. All the vectors are normalized to unit length. With these vectors, the weight for the body reflection is described as the inner product $(N \cdot L)$ or $(\cos$ ϕ), with ϕ being the angle of incidence.

On the other hand, the interface reflection is mirror-like, and the reflected light is observed within only a restricted range of the viewing angle. This reflection component is strongest in the direction of \mathbf{R}_1 , and it falls off sharply as the angle ρ between \mathbf{R}_1 and \mathbf{V} increases. This rapid falloff is often approximated by $(\cos \rho)^n$, where the index n is a measure of surface roughness. A small value of n provides a broad and gentle falloff, whereas a large value approximates a sharp and focused highlight. Moreover, if the highlight has a pointed peak, we may use $\exp(-n \mid \rho \mid)$ or $\exp(-n \mid \rho^2)$ for modeling the sharp falloff.

Combining the above geometric weights with the spectral components, the relative spectral distribution $Y(\theta,\lambda)$ of light reflected from an inhomogeneous dielectric object is described as

$$Y(\theta, \lambda) = f(\rho) S_I E(\lambda) + (\cos \phi) S_B(\lambda) E(\lambda), \tag{8}$$

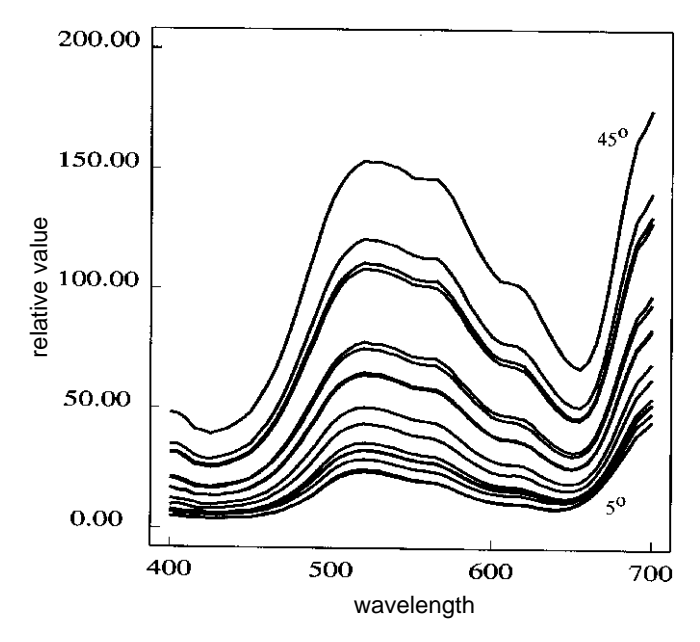


Figure 6. Surface-spectral reflectances observed from a green cloth of rayon satin.

where S_I is a constant value, and the specular attenuation function $f(\rho)$ may be chosen as $(\cos \rho)^n$, $\exp(-n \mid \rho \mid)$, or $\exp(-n \rho^2)$. The constant π is neglected. The model of Eq. 8 with $f(\rho) = (\cos \rho)^n$ corresponds to the Phong model widely used in computer graphics.

Type II Model. The extended model allows the interface reflection component to be a function of wavelength. The model equation is described by use of a wavelength-dependent function $S_I(\lambda)$ similar to that for Type I as

$$Y(\theta, \lambda) = f(\rho) S_{I}(\lambda) E(\lambda) + (\cos \phi) S_{R}(\lambda) E(\lambda), \qquad (9)$$

where the specular attenuation function $f(\rho)$ is selected as $(\cos \rho)^n$, $\exp(-n \mid \rho \mid)$, or $\exp(-n \rho^2)$.

Let us show an example for determining the specular term. Figure 6 shows the surface-spectral reflectances observed from a green cloth of rayon satin. The illumination was incident at a fixed angle of $\phi=45^\circ$. The viewing angle was varied from 5° to 45° of the mirrored direction. Reflectance was observed in the 5° to 35° range at 5° increments and in the 35° to 45° range at 1° increments. The spectral reflectance curves in Fig. 6 are not normalized; instead, they are depicted on a relative scale, where the spectral curve at the mirrored direction $\phi=45^\circ$ indicates a wavelength-dependent, high-reflectance function. This curve corresponds to $S_I(\lambda)$. On the other hand, the curve at $\phi=5^\circ$ is close to $S_B(\lambda)$. All the observed spectral reflectances can be expressed as linear combinations of these two curves.

Figure 7 depicts the averages of the observed spectral reflectances as a function of angle $\rho.$ For convenience, the averages are normalized to the maximum value of one at the highlight peak. The curve marked with plus symbols shows the variation as a function of $\rho.$ The curve marked with square symbols indicates the result of fitting the function $f(\rho) = \exp(-10 \mid \rho \mid)$ to the measurements, with ρ in radians. A comparison of the two curves suggests a good coincidence around the specular highlight in a range less than 10° from the peak.

Type III Model. Metal surfaces are not necessarily smooth, but rather rough in comparison with plastics. To determine the specular reflection function for such rough surfaces, the surfaces are idealized as being composed of

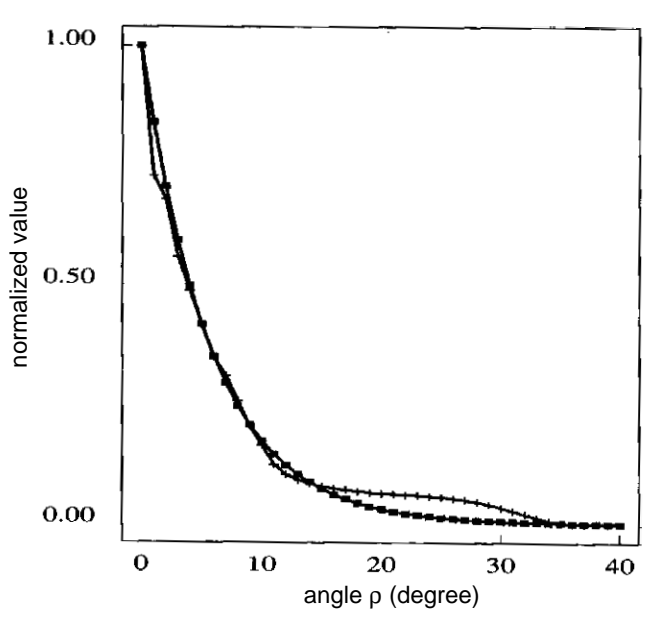


Figure 7. Normalized averages of the observed spectral reflectances and the fitting result as a function of angle ρ . Values indicated by plus symbols represent the averages. Squares represent the result of fitting $\exp(-10 |\rho|)$ to the data with ρ in radians.

small planar surface patches called *microfacets*. Based on this idealization, Torrance and Sparrow¹⁵ developed a physics-based model. Blinn² was the first to adapt their model to computer graphics. Cook and Torrance³ approximate the spectral composition of the specular reflection function in an implementation of their model. In this study, we apply the Torrance–Sparrow model to specify the geometric factor in the dichromatic reflection model.

In the Torrance–Sparrow model, the surface is assumed to be an isotropic collection of microfacets, each of which is a perfect smooth reflector. Figure 8 shows the reflection geometry for this case, where ${\bf H}$ is the vector bisector of an ${\bf L}$ and ${\bf V}$ vector pair, and ${\boldsymbol \alpha}$ is the angle between ${\bf H}$ and ${\bf N}$. The geometry and distribution of the microfacets and the direction of the incident light determine the intensity and direction of specular reflection. This specular reflection function is given by

$$Y(\theta, \lambda) = \frac{D(\alpha)G(\mathbf{N}, \mathbf{V}, \mathbf{L})}{\mathbf{N} \cdot \mathbf{V}} S(\theta, \lambda) E(\lambda), \tag{10}$$

where D is the distribution function of the microfacet orientation, G is the geometrical attenuation factor representing the mutual masking and shadowing effects of the microfacets, and S represents the spectral reflectance of the surface microfacets.

Function D describes the percentage of surface microfacets with normals oriented in the \mathbf{H} direction. Torrance and Sparrow assumed a Gaussian distribution function for D with rotational symmetry about the surface normal \mathbf{N} as

$$D(\alpha) = \exp\left\{-\ln(2)\alpha^2 / \beta^2\right\}, \tag{11}$$

where α is the angle shown in Fig. 8 and β is a constant. This constant β represents the angle for which the function value drops to 1/2.

Function G describes the fraction of the microfacets that are oriented in such a way that they are visible to both the light source and the viewer. Blinn discussed the

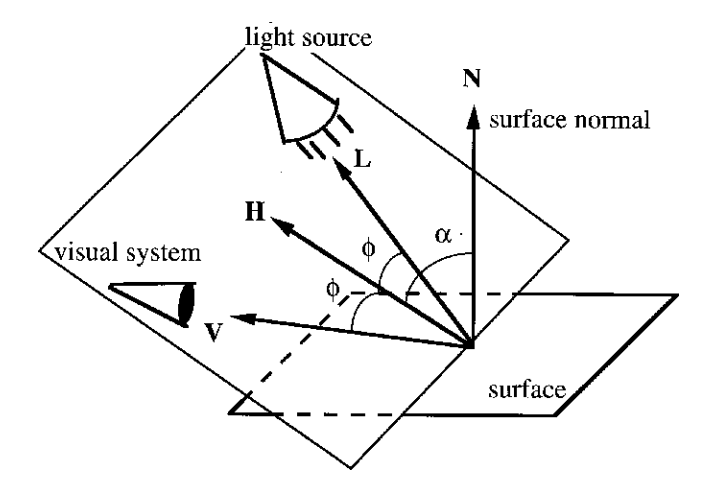


Figure 8. Reflection geometry for the Torrance-Sparrow model.

calculation of G for three different cases. In the first case, there is no interference, so that the incident light into a microfacet is totally reflected. In the second case, a microfacet is fully exposed to the rays, but some of the reflected rays are shielded by other microfacets. In the third case, a microfacet is partly shielded from the light. The function G ranges from 0 (total shadowing) to 1 (no shadowing) and takes minima in the three cases. The resulting attenuation function is given by

$$G(\mathbf{N}, \mathbf{V}, \mathbf{L}) = \min \bigg\{ 1, \frac{2(\mathbf{N} \cdot \mathbf{H})(\mathbf{N} \cdot \mathbf{V})}{(\mathbf{V} \cdot \mathbf{H})}, \frac{2(\mathbf{N} \cdot \mathbf{H})(\mathbf{N} \cdot \mathbf{L})}{(\mathbf{V} \cdot \mathbf{H})} \bigg\}. (12)$$

Because specular reflection occurs when light encounters an interface between the air and a metal surface, the spectral reflectance S can be computed theoretically from the Fresnel equations. The Fresnel equations are a solution to the Maxwell equations for electromagnetic wave behavior at a smooth interface between two homogeneous materials.¹⁷ The Fresnel equations are well defined and easy to put into code. However, the most severe obstacle to their general use is the lack of material information needed for the equations. Many optical material constants are included as parameters in the equations. For instance, although both the index of refraction and the absorption coefficient are required, these constants are often unknown except for some special compositions of typical metals. Cook and Torrance³ were the first to present an approximation method by neglecting the absorption constant and using the Fresnel equations for an inhomogeneous dielectric material. Hall¹⁸ presented an alternative method based on linear interpolation. These approximations use the spectral reflectance measurements at normal incidence $\phi = 0$ for estimating the missing optical constants.

In the present study we propose an effective method for estimating spectral reflectance at any incidence angle $(0<\phi<\pi/2)$ on the basis of the dichromatic reflection property. The method interpolates the measured reflectances without using any optical constants. Because the dichromatic model of Type III consists of the two components of the specular reflectance at normal incidence and the constant reflectance at grazing, the spectral reflectance is estimated by interpolating these two extreme reflectances. The interpolation equation is given as the weighted mean

$$S(\theta,\lambda) = \left(\frac{1-S_a(\phi)}{1-S_a(0)}\right) S_I(\lambda) + \left(\frac{S_a(\phi)-S_a(0)}{1-S_a(0)}\right), \quad (13)$$

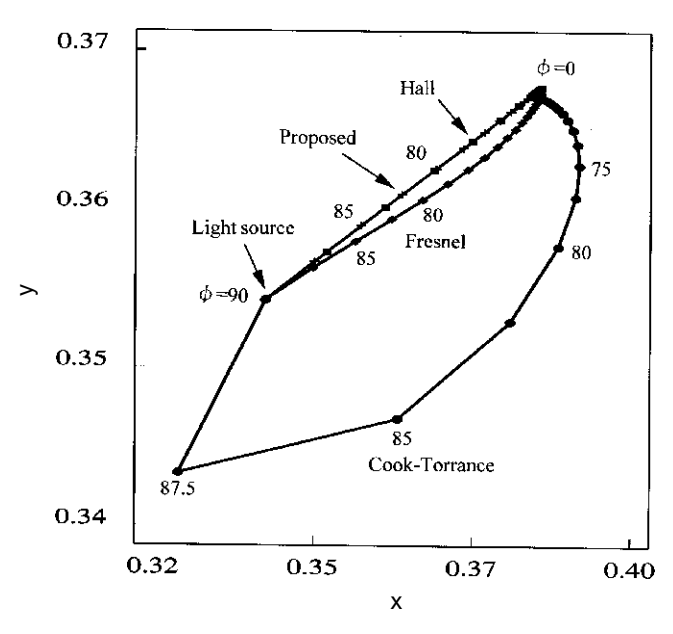


Figure 9. Chromaticity loci of four kinds of copper colors due to varying the incident angle. Diamonds represent the Fresnel locus. Plus symbols, squares, and circles represent, respectively, the proposed method, Hall's method, and the Cook-Torrance method for reflectance estimation.

where $S_a(\phi)$ is the average of the spectral reflectance for light incident at ϕ . This scalar $S_a(\phi)$ is obtained from reflectance measurements.

Let us show the validity of the above method for estimating metal spectral reflectance. The spectral reflectances obtained from the Fresnel equations for copper are used as the test data. We use the optical constants of the index of refraction and the absorption coefficient from Ref. 19. The color of the reflected light from this copper varies with the angle of incidence of illumination. Figure 9 shows a plot of the chromaticity loci of four kinds of copper color on an *xy* chromaticity diagram for the copper surface being illuminated with sunlight at different angles of incidence. As the incident angle approaches 90°, the copper color's saturation drops, that is, it approaches the color of the light source. First we note that there is a huge chromaticity discrepancy between the Cook-Torrance method and the Fresnel locus at a wide range of angles above 70°. Next we note that the present method based on Eq. 13 and Hall's method vary linearly. These loci approximate the Fresnel chromaticity locus. Moreover, a detailed comparison of chromaticity points on the two straight loci shows that chromaticity differences between the points marked with plus symbols and the points marked with diamonds at the respective incidence angles around 80° to 90° are much smaller than the differences between the points marked with squares and the points marked with diamonds. Thus, the present method (marked with plus symbols) provides a good approximation of the Fresnel reflectance over the whole range of the incidence angle.

Applications

Sample images are generated on the basis of the above models for three different materials. We use a ray-tracing technique for rendering a computer graphics scene of three-dimensional objects, ²⁰ where the visible surfaces in a scene are mapped to a screen image by ray tracing. Then the color for each pixel of the image is determined by spectral computation as follows: First the spectral



 $\textbf{Figure 10.} \ \textbf{Generated image of blue and red cups made of an inhomogeneous dielectric material.}$

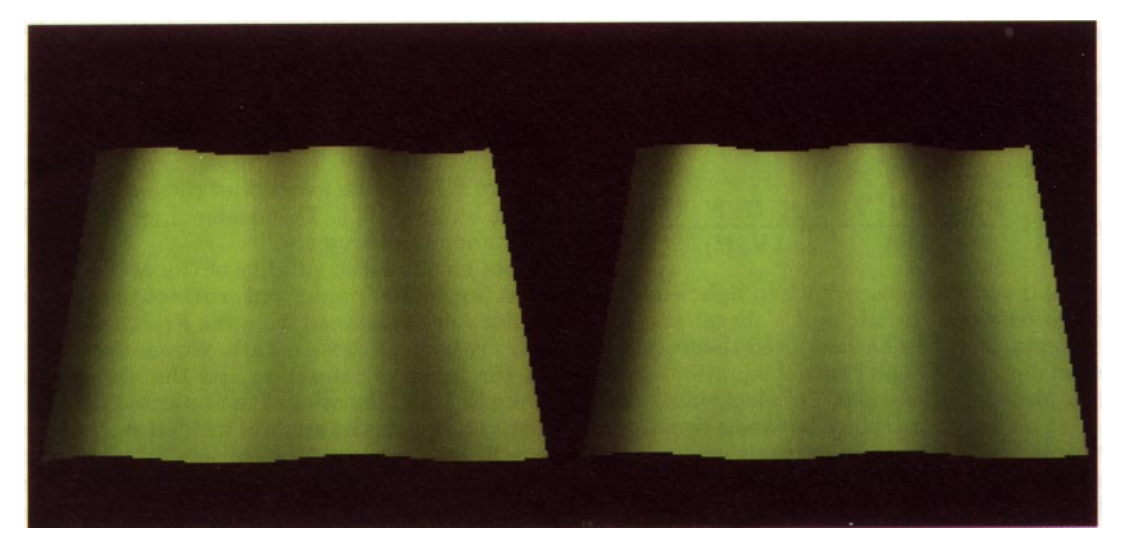
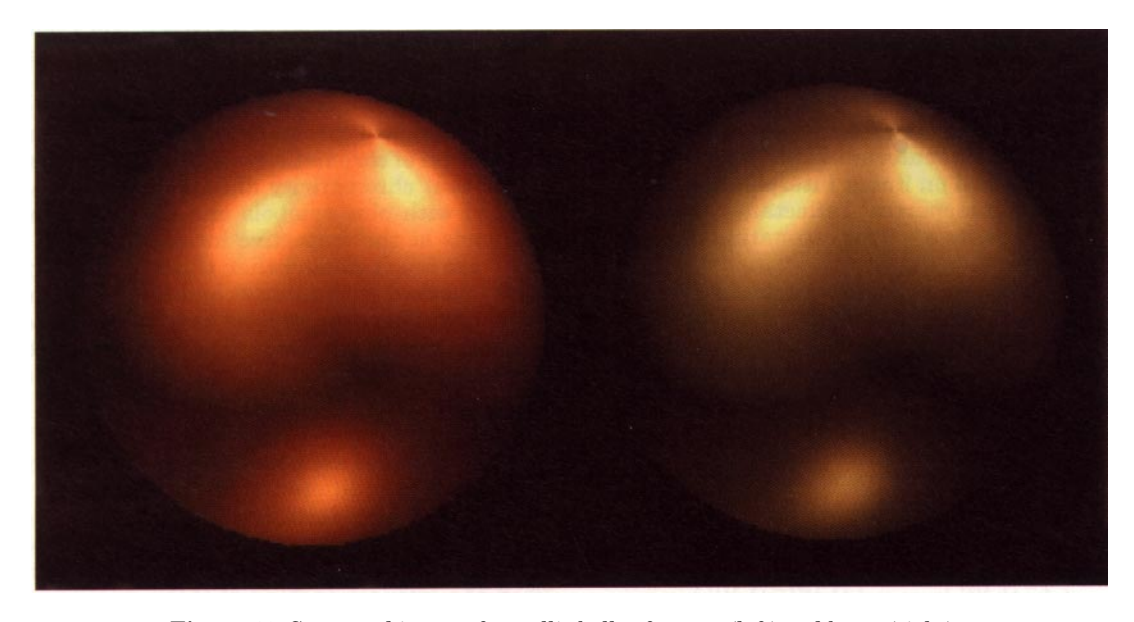


Figure 11. Generated image of green cloths for two views in vertical and horizontal directions.



 $\textbf{Figure 12.} \ Generated \ image \ of \ metallic \ balls \ of \ copper \ (left) \ and \ brass \ (right).$

power distribution of light reflected from object surfaces is computed over the visible wavelength range, 400 to 700 nm. All spectra are sampled at 5 nm intervals for the description as 61 dimensional vectors. After the spectral radiant computation, the pixel's color is determined in terms of the tristimulus values CIE-XYZ. Finally the image is displayed on a calibrated CRT monitor. For exact color reproduction, the tristimulus values are converted into the monitor RGB values by a transformation matrix, and gamma correction is applied through lookup tables. The image is also printed on a color printer. Neural network computation is used for the conversion of the color stimuli into the CMYK printer ink signals.²¹

Figure 10 is the image of a blue cup and a red cup generated with the Type I model for inhomogeneous dielectric materials. The cup material looks like plastic. Cones, cylinders, and spheres are used as the primitive objects for geometric modeling of each cup. Spectral measurement data are used for the surface-spectral reflectances $S_B(\lambda)$ and the illuminant spectrum $E(\lambda)$. The light source is assumed to be the point source of a slide-projector lamp. The parameters in Eq. 8 are set to $f(\rho) = (\cos \rho)^{11}$ and $S_I = 5$.

Figure 11 is the image of green cloths generated with the Type II model. Many triangular patches are used for forming the smooth cloth surfaces. The two spectralreflectance functions $S_R(\lambda)$ and $S_I(\lambda)$ are determined as the two extreme spectral curves of rayon satin at 5° and 45°, as shown in Fig. 6. The spectral reflectances differ a little with the viewing direction of the texture. The two images in Fig. 12 were generated for viewpoints lying in the vertical and horizontal directions. The attenuation function is $f(\rho) = \exp(-10 |\rho|)$. The light source is a point source D_{65} .

Figure 12 is the image of metallic balls of copper (left) and brass (right) generated with the Type III model. For the surface-spectral reflectance estimation, the proposed interpolation method was applied to the measured reflectances of plates of both copper and brass. The constant in Eq. 11 is $\beta = 5^{\circ}$, but the Torrance–Sparrow model has been modified slightly because the effect of anisotropic reflection was added to realize more realistic appearance. Spin finish is effective for simulating the burnished metal surface whose microfeatures are preferentially oriented. Each ball is illuminated by three directional D_{65} light sources, whose rays all come from the same direction (such as the distant sun).

Conclusion

This paper has described light reflection models adequate for generating realistic images of reflective object surfaces of different materials. First we showed three types of dichromatic reflection models for describing surface-spectral reflectances of a variety of materials. Next we determined the geometric factors of illumination and viewing, which had previously been left undetermined as the weighting coefficients to the spectral components in the dichromatic reflection models. The intensity distribution of the reflected light from a surface is formulated by referring to reflection models in computer graphics. The Type I model for objects of inhomogeneous dielectric materials assumes that surface reflection consists of two additive components, the body reflection and the interface reflection, which is independent of wavelength. The Type II model allows wavelength-dependent interface reflection that is adequate for cloths and papers. The Type III model is specialized for the specular reflection only and is used for describing metallic objects. Reflective object surfaces of most materials can be rendered using these three types of the dichromatic model. Finally, sample images for different surface types were generated. The validity of the models is confirmed by comparing the generated images with the real objects.

References

- B. T. Phong, Illumination for computer-generated pictures, Comm. ACM, 18: 311 (1975).
- J. F. Blinn, Model of light reflection for computer synthesized pictures, Computer Graphics, 11: 192 (1977).
- R. L. Cook and K. E. Torrance, A reflection model for computer graphics, Computer Graphics, 15: 307 (1981).
- G. J. Klinker, S. A. Shafer, and T. Kanade, The measurement of highlights in color images, Int. J. Computer Vision, 2:147 (1988).
- G. Healey, Using color for geometry-insensitive segmentation, J. Opt. Soc. Amer. A, 6: 920 (1989).
- A. G. Maristany et al., Classifying wood-surface features using dichromatic reflections, SPIE Symp. Optics in Agriculture and Forestry, Boston,
- M. S. Drew. Optimization approach to dichromatic images. J. Math. Imaging Vision, 3: 187 (1993).
- S. Tominaga, Realization of color constancy using the dichromatic reflection model, 2nd IS&T/SID Color Imaging Conf., 1994, p. 37.

 N. Usui and A. Imamura, Printing simulator, TAGA Symp., Paris, 1995.
- S. Shafer, Using color to separate reflection components, Color Res. Appl., 10: 210 (1985).
- S. Tominaga and B. A. Wandell, The standard surface reflectance model and illuminant estimation, J. Opt. Soc. Amer. A, 6: 576 (1989).
- H. C. Lee, E. J. Breneman, and C. Schulte, Modeling light reflection for computer color vision, IEEE Trans. Patt. Anal. Mach. Intell, 12: 402 (1990)
- S. Tominaga, Dichromatic reflection models for a variety of materials, Color Research and Application, 19: 277 (1994).
- G. Wyszecki and W. S. Stiles, Color Science, 2nd ed., John Wiley & Sons, New York, 1982.
- K. E. Torrance and E. M. Sparrow, Theory for off-specular reflection from roughened surfaces, J. Opt. Soc. Am., 57: 1105 (1967)
- P. Burger and D. Gillies, Interactive Computer Graphics, Addison-Wesley, Reading, MA, 1989, p. 305.
- M. Born and E. Wolf, Principles of Optics, Pergamon Press, Oxford,
- R. Hall, Illumination and Color in Computer Generated Imagery, Springer-Verlag, Berlin, 1989.
- D. Palik (Ed.), Handbook of Optical Constants of Solids, Academic Press, San Diego, 1985.
- J. D. Foley, A. van Dam, S. K. Feiner, and J. F. Hughes, Computer Graphics, 2nd ed., Addison-Wesley, Reading, MA, 1990, p. 701.
- S. Tominaga, Color control using neural networks and its application, Proc. SPIE, 2658: 253 (1996).